American Mineralogist, Volume 89, pages 681–695, 2004

Evidence for exclusively inorganic formation of magnetite in Martian meteorite ALH84001

D.C. GOLDEN,[1] D.W. MING,[2,*] R.V. MORRIS,[2] A.J. BREARLEY,[3] H.V. LAUER JR.,[4] A.H. TREIMAN,[5] M.E. ZOLENSKY[2], C.S. SCHWANDT,[4] G.E. LOFGREN,[2] AND G.A. MCKAY[2]

[1]Hernandez Engineering Inc., 16055 Space Center Boulevard, Suite 725, Houston, Texas 77062, U.S.A.
[2]Astromaterials Research and Exploration Science Office, Mail Code SA13, NASA Johnson Space Center, Houston, Texas 77058, U.S.A.
[3]Department of Earth and Planetary Sciences, University of New Mexico, Albuquerque, New Mexico 82131-1126, U.S.A.
[4]Lockheed Martin, Mail Code C23, P.O. Box 58561, Houston, Texas 77258-8561, U.S.A.
[5]Lunar and Planetary Institute, 3600 Bay Area Boulevard, Houston, Texas 77058-1113, U.S.A.

ABSTRACT

Magnetite crystals produced by terrestrial magnetotactic bacterium MV-1 are elongated on a [111] crystallographic axis, in a so-called "truncated hexa-octahedral" shape. This morphology has been proposed to constitute a biomarker (i.e., formed only in biogenic processes). A subpopulation of magnetite crystals associated with carbonate globules in Martian meteorite ALH84001 is reported to have this morphology, and the observation has been taken as evidence for biological activity on Mars. In this study, we present evidence for the exclusively inorganic origin of [111]-elongated magnetite crystals in ALH84001. We report three-dimensional (3-D) morphologies for ~1000 magnetite crystals extracted from: (1) thermal decomposition products of Fe-rich carbonate produced by inorganic hydrothermal precipitation in laboratory experiments; (2) carbonate globules in Martian meteorite ALH84001; and (3) cells of magnetotactic bacterial strain MV-1. The 3-D morphologies were derived by fitting 3-D shape models to two-dimensional bright-field transmission-electron microscope (TEM) images obtained at a series of viewing angles. The view down the {110} axes closest to the [111] elongation axis of magnetite crystals ([111]·{110} ≠ 0) provides a 2-D projection that uniquely discriminates among the three [111]-elongated magnetite morphologies found in these samples: [111]-elongated truncated hexa-octahedron ([111]-THO), [111]-elongated cubo-octahedron ([111]-ECO), and [111]-elongated simple octahedron ([111]-ESO). All [111]-elongated morphologies are present in the three types of sample, but in different proportions. In the ALH84001 Martian meteorite and in our inorganic laboratory products, the most common [111]-elongated magnetite crystal morphology is [111]-ECO. In contrast, the most common morphology for magnetotactic bacterial strain MV-1 is [111]-THO. These results show that: (1) the morphology of [111]-elongated magnetite crystals associated with the carbonate globules in Martian meteorite ALH84001 is replicated by an inorganic process; and (2) the most common crystal morphology for biogenic (MV-1) magnetite is distinctly different from that in both ALH84001 and our inorganic laboratory products. Therefore, [111]-elongated magnetite crystals in ALH84001 do not constitute, as previously claimed, a "robust biosignature" and, in fact, an exclusively inorganic origin for the magnetite is fully consistent with our results. Furthermore, the inorganic synthesis method, i.e., the thermal decomposition of hydrothermally precipitated Fe-rich carbonate, is a process analogue for formation of the magnetite on Mars. Namely, precipitation of carbonate globules from carbonate-rich hydrothermal solutions followed at some later time by a thermal pulse, perhaps in association with meteoritic impact or volcanic processes on the Martian surface.

INTRODUCTION

Magnetite crystals in Martian meteorite ALH84001 are a focus of controversy about the possibility of past (and present) life on Mars. McKay et al. (1996) suggested that some magnetite crystals associated with carbonate globules in the meteorite are biogenic because they share many characteristics with magnetosomes from terrestrial magnetotactic bacteria. These characteristics include: size consistent with single magnetic domains, absence of crystalline defects, chemical purity, and coexistence with metastable phases in apparent disequilibrium. Thomas-Keprta et al. (2000) showed that a subpopulation (~27%) of the magnetite crystals in ALH84001 carbonate globules has a crystal habit characterized by elongation on a [111] crystallographic axis. The "unique habit" of the population was claimed to be identical to that of magnetite grains produced by the terrestrial magnetotactic bacterium MV-1. Thomas-Keprta et al. (2001, 2002) use the name "truncated hexa-octahedron" to describe this morphology, which we abbreviate to "[111]-THO." Thomas-Keprta et al. (2002), drawing upon the earlier papers (e.g., McKay et al. 1996; Thomas-Keprta et al. 2000, 2001), concluded that the [111]-THO morphology (by analogy with MV-1) and the aforementioned properties of biogenic magnetite are evidence for a biogenic origin for the [111]-elongated subpopulation of magnetite in ALH84001.

* E-mail: douglas.w.ming@nasa.gov

In this paper, we investigate two claims from Thomas-Keprta et al. (2001, 2002) that are critical to their conclusion that a subpopulation of magnetite crystals in ALH84001 are biogenic. First, we investigate whether a reasonable inorganic process can produce magnetite crystals identical to those in ALH84001 purported to be biogenic. If an inorganic process can produce such magnetite crystals, the claim of a biological origin is greatly weakened. Second, we seek to replicate a fundamental tenet of the McKay et al. (1996) hypothesis—that the purported biogenic sub-population of magnetite grains in ALH84001 is identical to those produced by the bacterium MV-1. Anticipating our conclusions, we have found that thermal decomposition of Fe-bearing carbonate produces magnetite crystals that are identical to those found in ALH84001. Moreover, we have found that most of the purported biogenic magnetite crystals in ALH84001 do not have the reported [111]-THO morphology, and so are not identical to those from the MV-1 bacterium. These results together cast serious doubt on the hypothesis that any magnetite crystals in ALH84001 are biogenic and provide strong evidence for an exclusively inorganic origin.

Nomenclature

The discussion of magnetite crystals and their possible biogenic origin is plagued by confusing and inconsistent nomenclature for the shapes of submicrometer magnetite crystals that are elongated on a [111] direction. Throughout this manuscript "(*hkl*)" will denote a face, "{*hkl*}" will denote a form, and "[*hkl*]" will denote a zone axis. Faces and axes of a form will be denoted as "{*hkl*} faces" and "{*hkl*} axes," respectively. Central to the arguments developed in this paper is a clear understanding of the "truncated hexa-octahedral" morphology. This shape is defined as having eight {111} octahedral faces, six {110} hexagonal faces parallel to the elongation direction, and six {100} cubic faces (Thomas-Keprta et al. 2001). The six {110} "hexagonal" faces belong to the [111] zone (i.e., [111]·{110} = 0). The "truncated hexa-octahedron" nomenclature is confusing because it refers to the six hexagonal {110} faces (see Fig. 1 in Thomas-Keprta et al. 2001), which are actually dodecahedral faces. The confusion is extended in the phrase "hexa-octahedron coccoid" (see Fig. 4 C1-C3 in Thomas-Keprta et al. 2001) to describe similar crystals that express all 12 dodecahedral faces. Nevertheless, the name "[111]-THO" is used here to facilitate discussion within the context of Thomas-Keprta et al. (2001) and related papers.

Geologic history of ALH84001

ALH84001 has experienced a complex history of repeated deformation and shock-metamorphic events (Treiman 1995, 1998, 2001, 2003), providing several opportunities for shock metamorphism in ALH84001 carbonates. It has been proposed that the magnetite in ALH84001 carbonate globules formed by thermal decomposition of Fe-bearing carbonate during one of these shock events (Brearley 1998; Bradley et al. 1998; Kring et al. 1998; Golden et al. 2001, 2002; Koziol and Brearley 2002; Barber and Scott 2002, Treiman 2003). Another product of thermal decomposition of carbonates, periclase (MgO), has been reported in ALH84001 (Barber and Scott 2002) and so has its hydration product brucite (Treiman and Keller 2000).

A critical aspect of thermal decomposition processes is the relationship among carbonate decomposition temperatures. In general, Fe-rich carbonate decomposes to magnetite at lower temperatures than either Mg-rich or Ca-rich carbonates decompose to their respective oxides (Treiman 2003). This simple relation is complicated by the fact that decomposition of Fe carbonate (siderite) is a function of oxygen fugacity: $3FeCO_3 \rightarrow Fe_3O_4 + CO + 2CO_2$. Because Fe-Mg carbonates (like those abundant in ALH84001) form a continuous solid-solution series, heating to a given temperature will decompose only those carbonates more ferroan than some limiting value, which can be calculated from thermochemical data (Treiman 2003).

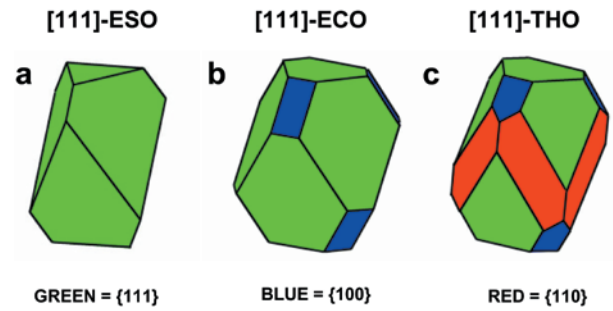

FIGURE 1. Common elongated magnetite crystal morphologies of synthetic crystals formed by the thermal decomposition of Fe-rich siderite, crystals in Martian meteorite ALH84001, and crystals produced by magnetotactic bacteria strain MV-1. (**a**) [111]-elongated simple octahedron ([111]-ESO) has eight {111} faces and is elongated along the [111] direction. **(b)** [111]-elongated cubo-octahedron ([111]-ECO) has eight {111} and six {100} faces (all {100} faces equivalent) and is elongated along the [111] direction. (**c**) [111]-truncated hexa-octahedron ([111]-THO) is defined by Thomas-Keprta et al. (2001) as a magnetite morphology with eight {111}, six {110}, and six {100} faces, and is elongated along the [111] direction. The green, blue, and red colors denote the {111}, {100}, and {110} faces, respectively.

Precursor experiments

To understand the formation and thermal decomposition of the ALH84001 carbonates, Golden et al. (2000a, 2000b, 2001) precipitated chemically zoned and sulfide-bearing carbonate globules analogous to those in ALH84001 (at ≤150 °C) from multiple fluxes of variable-composition Ca-Mg-Fe-CO_2-S-H_2O solutions. Magnetite was a minor precipitate with the carbonate globules when the Eh and Fe^{2+} activity were sufficiently high (see Table 1 in Golden et al. 2000a). Brief heating of the precipitated globules to approximately 470 °C produced magnetite and pyrrhotite within the globules by thermal decomposition of siderite and pyrite, respectively (Golden et al. 2001). This heating caused neither ankerite cores nor magnesite rims of the globules to decompose, except in rare instances. Magnetite crystals produced by thermal decomposition in these experiments have a narrow size distribution in the single domain to superparamagnetic range, are chemically pure and free of structural defects, and many have elongation along the [111] crystallographic axis.

Golden et al. (2001) did not study the shapes of these thermal decomposition magnetite crystals in detail—that is the focus of the present work. We characterize here the three-dimensional (3-D) shapes of magnetite crystals produced during the thermal decomposition of hydrothermally produced siderite and Mg-

siderite assemblages. The 3-D shapes of the magnetite crystals were determined by multiple TEM bright-field images, extending the method of Thomas-Keprta et al. (2001). We also present new data on the shapes of magnetite crystals from ALH84001 and biogenic magnetite crystals from MV-1. Hence, we directly compare [111]-elongated morphologies for samples where biogenic origin is certain (MV-1), where inorganic origin is certain (our inorganic synthesis products), and where the origin is under question (Martian meteorite ALH84001).

Experimental methods

Inorganic magnetite synthesis

Inorganic magnetite was produced by the thermal decomposition of hydrothermally precipitated Fe-rich carbonate. Fe-Mg-bicarbonate solutions were prepared by mixing 40 m*M* aqueous $FeCl_2{\cdot}4H_2O$ solutions with 1 *M* $MgCl_2{\cdot}6H_2O$ solutions to give solutions with 2 and 75 mol% Mg. A solution of 1 *M* $NaHCO_3$ was then added under a CO_2 purge (Golden et al. 2000a, 2000b, 2001). Aliquots (15 mL) from each resultant Fe-Mg bicarbonate solution were heated individually at 150 °C for 7 h in a sealed Teflon-lined stainless steel reaction vessel. Carbonate globules were removed from the vessels and washed with de-ionized water to remove soluble salts (e.g., NaCl), dried, and placed in a 1-bar gas-mixing furnace with CO_2:CO = 95:5. The temperature was ramped at 60 °C/h to 550 °C, held at temperature for 1 h, and then cooled at 200 °C/h to ambient temperature. Some magnetite crystals co-precipitate during the hydrothermal precipitation of siderite. The amount of precipitated magnetite was controlled by the Eh of the solution, which, in turn, depended mainly on Fe^{2+} activity and P_{O_2}. The majority of the magnetite is formed during thermal decomposition of siderite (see discussion below). The morphological characteristics of magnetite that formed from siderite were independent of the Mg content of the starting solutions (2 and 75 mol% Mg). Because the morphological properties were similar, only the morphological data for the magnetite formed from 2 mol% Mg starting solutions will be presented here.

Mineralogical properties of products from both the hydrothermal precipitation (150 °C) and thermal decomposition (550 °C) steps were characterized by X-ray diffraction (XRD) analysis. A Scintag XDS 2000 X-ray diffractometer using Cu$K\alpha$ radiation operated at 45 kV and 40 mA current was used to analyze random powder mounts over the range of 2–70° 2θ.

Extraction of magnetite from inorganic synthesis experiments

Magnetite crystals were separated from the heated carbonate globules using a procedure modified from Thomas-Keprta et al. (2000). The products were treated with 1 mL of 20% acetic acid at 65 °C for 72 h, followed by a second dissolution if necessary to remove remaining carbonate. The acid extract containing the magnetite was spun in a Fisher Microcentrifuge at 13 900 g for 5 min. The supernatant was transferred to a 100 mL volumetric flask using a micropipette, and the residue was washed five times with distilled water (solid:solution = 1:200) by suspension and centrifugation.

After extraction, the magnetite crystals were dispersed ultrasonically in distilled water and transferred onto a carbon substrate over a Cu-grid with a pole of a C-shaped magnet placed below the grid. This sample preparation technique produced linear strands of well-separated magnetite crystals along the magnetic lines of force. TEM examination of magnetite before and after the acetic acid extraction indicates that the acid extraction technique did not alter the size and shape of magnetite crystals.

Magnetite crystals were examined at 160 or 200 kV with a JEOL 2000FX transmission electron microscope (TEM) equipped with a Link System IV energy-dispersive X-ray spectrometer (EDS) (Johnson Space Center) and at 200 kV with a JEOL 2010 TEM equipped with a Gatan slow scan CCD camera (University of New Mexico). Double tilt sample holders with ±45° tilt in each direction were used for orienting samples in the TEM. EDS spectra were collected with sufficient counts so that the uncertainty on the basis of statistics was <3% for major elements. EDS detection limits (Joy et al. 1986) are ~0.3 wt% for Mg and ~0.5 wt% for Fe unless otherwise stated.

Extraction of magnetite from ALH84001 and MV-1

Pancake-shaped ALH84001 carbonate globules with double black rims containing magnetite were carefully chipped away from the orthopyroxene (Opx) matrix leaving as little adhering Opx as possible. The magnetite crystals were extracted from the carbonates and then mounted on a C-substrate on Cu-grids for TEM analysis as described above.

Magnetite crystals still in MV-1 bacteria magnetosomes were treated with 5% sodium hypochlorite (Mann et al. 1987), washed free of salts, dispersed in water by ultrasonic dispersion, and mounted on a C-substrate on Cu-grids for TEM-EDS analyses. Some MV-1 crystals were directly dispersed for morphological analyses without oxidizing the magnetosome membranes.

Analytical methods: Magnetite crystal shape and size

Crystal morphology

The 3-D shape of each individual magnetite crystal was reconstructed from outlines of two-dimensional (2-D) TEM bright-field images of the crystal obtained at different tilt angles. Tilt angles ranged from ~ –45° to +45° at magnifications of 40 000–500 000. We studied a total of ~1000 magnetite crystals from all three types of samples. Each crystal was imaged at a minimum of 3 tilt positions to determine if it was elongated. If elongated, images at additional tilt directions were obtained to determine the elongation direction. Representative magnetite crystals from those elongated along the [111] crystallographic axis were examined further by electron diffraction and additional tilts. The projected 2-D TEM images of magnetite crystals at various tilts were compared to simulated projections of a series of 3-D polyhedral shapes that are generated by the JCrystal crystallography editor and viewer software (Weber 2000).

We found three specific morphologies for magnetite crystals elongated along the [111] axis: the [111]-elongated simple octahedron ([111]-ESO), the [111]-elongated cubo-octahedron ([111]-ECO), and the [111]-elongated truncated hexa-octahedron ([111]-THO) (Fig. 1). The [111]-ESO shape has only the eight {111} octahedral faces. The [111]-ECO shape has eight {111} octahedral faces and six {100} cubic faces. The [111]-THO shape has eight {111} octahedral faces, six {100} cubic faces, and six {110} rhombic dodecahedral faces parallel to the [111] elongation direction. Unfortunately, the outlines of 2-D projections in most zone-axis orientations (e.g., [100] and [111]) are insensitive to the presence or absence of the {110} faces that differentiate the [111]-THO and [111]-ECO shapes from each other. Similarly, the dihedral edges are indistinguishable from faces in some 2-D projections (e.g., [111]-THO and [111]-ESO down the [111] elongation axis).

This difficulty in distinguishing between the [111]-THO and [111]-ECO shapes in 2-D projections as observed by bright-field TEM imaging is apparent in Figure 2, which shows [111]-THO and [111]-ECO shape models in all possible orientations at 30° steps for both crystal shapes. Tilts are shown around the Y and Z axes; tilts around the X-axis (perpendicular to the plane of the paper) will only change angular positions and not alter the 2-D shapes. Only the perimeter outline of the 3-D shape models is readily apparent in 2-D projections. For most crystal orientations, the 2-D projections for the [111]-THO and [111]-ECO shapes are indistinguishable. However, [111]-THO and [111]-ECO can be reliably distinguished in the projection at Y = 60° and Z = 0°, which looks down one of the three {110} zone axes closest to the [111] elongation axis ([111]·{110}≠0). These directions will be denoted as $\{110\}_e$ (see Fig. 3a). As shown in Figure 3b, the [111]-THO projection down $\{110\}_e$ is an octagon (consisting of {111}, {100}, and {110} faces), the [111]-ECO projection is a hexagon (consisting of {111} and {100} faces, and the [111]-ESO projection is a rhombus (consisting of {111} faces).

Although a view down a $\{110\}_e$ direction is unambiguous in discriminating among [111]-ESO, [111]-ECO, and [111]-THO crystal shapes, it is a tedious test to implement. A TEM grid with magnetite crystals was inserted into the TEM on a double-tilt sample holder and we searched grain-by-grain for [111] elongated crystals that could be oriented properly at a $\{110\}_e$ axial view and also yield sharp uncluttered images in tilt sequences. Crystal orientations were confirmed by TEM selected-area electron diffraction (SAED) or by 2-D Fast Fourier Transforms (FFT) of TEM high-resolution lattice fringe images. We were able to obtain 2-D images at various tilts (plus and minus) around $\{110\}_e$ axes for 80 magnetite crystals (50 inorganic crystals, 26 MV-1 crystals, and 6 ALH84001 crystals). The relatively few crystals for ALH84001 reflects the few [111]-elongated crystals in our samples (see below).

Crystal size

For our inorganic synthesis experiments, we determined the crystal-size distribution for the magnetite crystals produced by thermal decomposition of siderite. We only considered those grains with no detectable Mg content that were produced

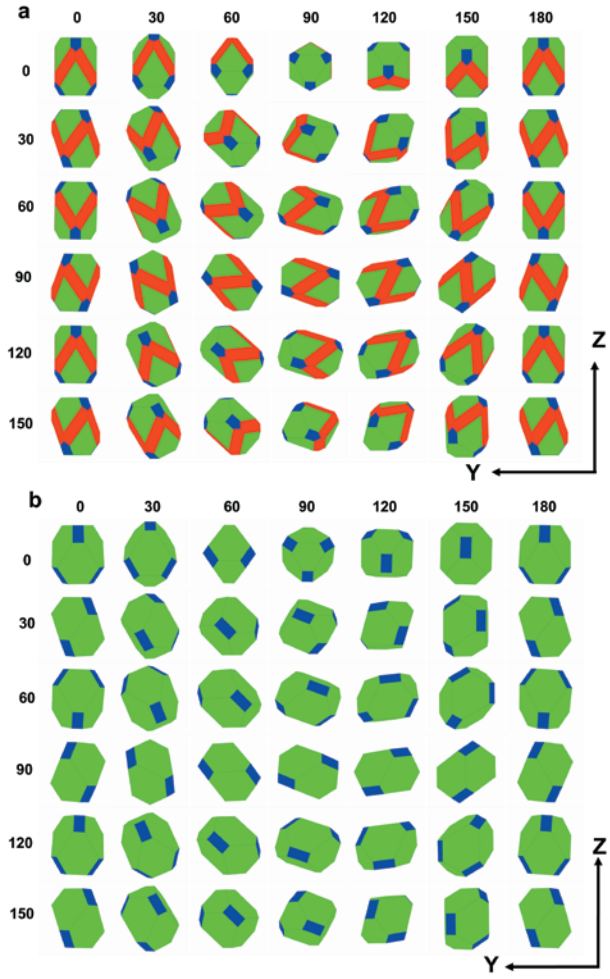

FIGURE 2. (**a**) [111]-THO crystal shape model in all possible orientations at 30° steps. Tilts are shown around Y and Z axes; tilts around the X axis (perpendicular to the plane of the paper) will not alter the 2-D shape but only its angular position. (**b**) [111]-ECO crystal shape model with the same orientation matrix. The green, blue, and red colors denote the {111}, {100}, and {110} faces, respectively.

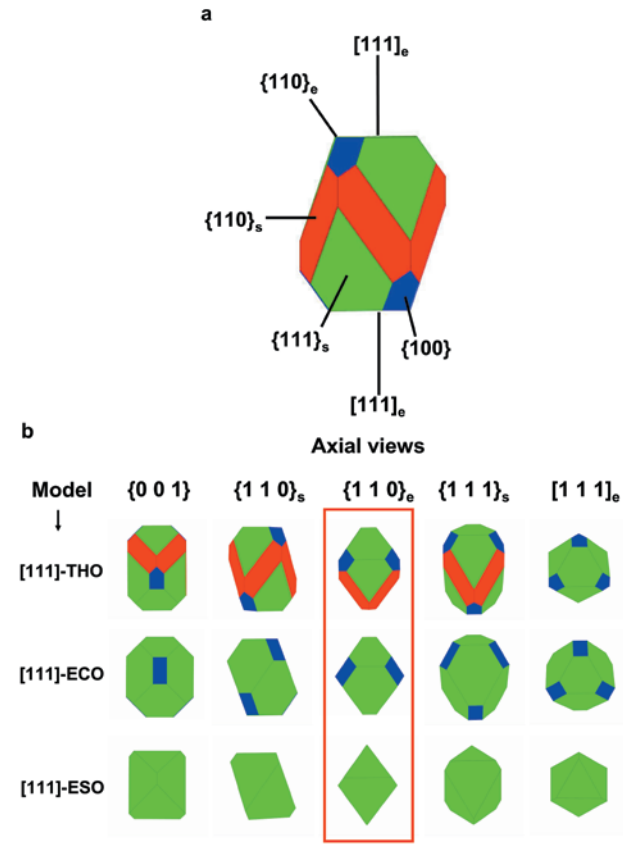

FIGURE 3. (**a**) Definition of elongated and short axes used in this study for the [111]-THO model (and [111]-ECO model without the {110} faces shown here): $\{110\}_s = \{110\}$ short axes, $\{110\}_e = \{110\}$ elongated axes, $\{111\}_s = \{111\}$ short axes, and $[111]_e = [111]$ elongated axis. Note that the orientation of this crystal corresponds to z=90 in Figure 2a. (**b**) Morphology models oriented down various zone axes that distinguish among the elongated magnetite morphologies for the [111]-THO, [111]-ECO, and [111]-ESO shaped models: {001}, $\{110\}_s$ where $[111]\cdot\{110\} = 0$ (i.e., orthogonal vectors), $\{110\}_e$ where $[111]\cdot\{110\}\neq 0$ (i.e., non-orthogonal vectors), $\{111\}_s$, and $[111]_e$. The 2-D shapes of the $\{110\}_e$ views for [111]-THO, [111]-ECO, and [111]-ESO are highlighted within the red box. Note that the 2-D shapes for the [111]-THO, [111]-ECO, and [111]-ESO are an octagon, hexagon, and rhombus, respectively.

from the 2 mol% Mg starting solutions. Magnetite crystal outlines regardless of shape were digitized from scanned low-magnification TEM photomicrographs (total of 578 randomly selected crystals of which 382 were [111] elongated). Their dimensions were determined by calculating the best fit of ellipses projected onto particle 2-D images. The ellipse major and minor axes lengths were taken as the observed crystal length and width. According to Devouard et al. (1998) and Thomas-Keprta et al. (2000), this procedure represents well the actual size of magnetite crystals. However, because only the major and minor axes of the ellipse are taken into consideration, the size parameters obtained this way are insensitive to the presence or absence of minor faces (including the {110} faces that distinguish the [111]-THO shape from the [111]-ECO shape).

RESULTS OF INORGANIC SYSTHESIS EXPERIMENTS

Carbonate mineralogical composition

Carbonate precipitates from mixed Mg-Fe-bicarbonate solutions consisted of zoned carbonate globules with Fe-rich cores and Mg-rich rims. XRD analyses show that the Fe-rich carbonate is siderite and the Mg-rich carbonate is magnesite. Although very high Mg concentrations (relative to Fe) were present in one of the mixed bicarbonate starting solutions (i.e., 75 mol% Mg), relatively little Mg was incorporated into the Fe-carbonate core. An EDS transect of a carbonate globule that formed from the high-Mg-starting solution (i.e., 75 mol% Mg) is shown in Figure 4. There is clearly an enrichment of Fe in the center of the globule and a steep gradient to Mg-rich carbonate in the rim. Such distinct zones of Fe-rich and Mg-rich carbonates are predicted in precipitation models for mixed Fe and Mg bicarbonate solutions under low-temperature hydrothermal conditions (Woods and Garrels 1992; Catling 1999). Golden et al. (2000a) have previously demonstrated these zonation sequences in laboratory experiments.

Magnetite formation pathways

Magnetite crystals formed by two pathways in our inorganic synthesis experiments: direct precipitation during hydrothermal synthesis (Golden et al. 2000a, 2001), and thermal decomposi-

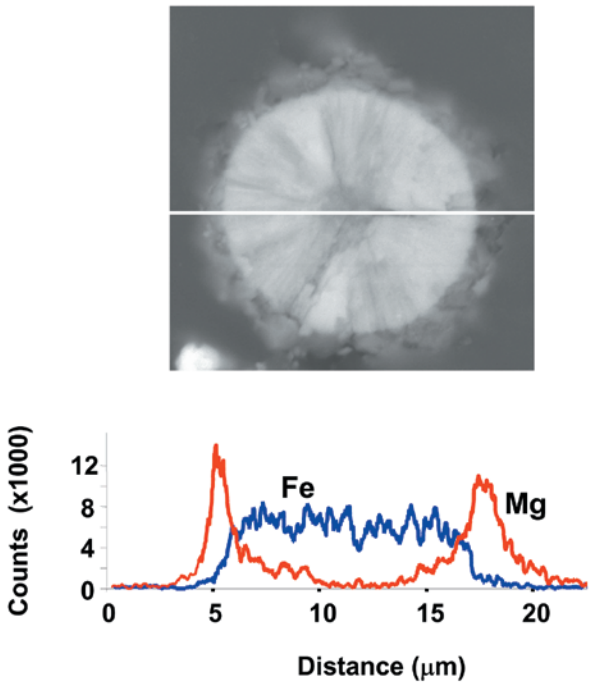

FIGURE 4. Distribution of Mg and Fe in synthetic Mg-Fe-carbonate globules precipitated from Mg and Fe bicarbonate hydrothermal solutions (75 mol% Mg and 25 mol% Fe starting solutions heated to 150 °C). The core of the globule is Fe-rich. The outer zone grades into nearly pure magnesite. The X-ray EDS transect was taken along the white line shown on the SEM back-scattered electron image.

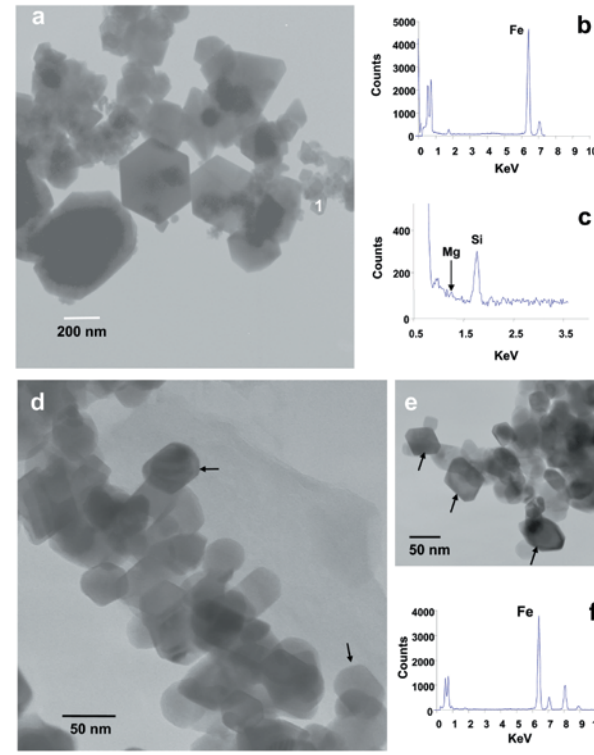

FIGURE 5. (**a**) TEM 2-D image of magnetite that precipitated along with carbonate globules from low-Mg hydrothermal solutions (150 °C). Note that many of the euhedral crystals have sharp corners. (**b**) X-ray EDS scan of particle 1 in Figure 5a that shows the crystal is free of Mg at >4000 total counts for Fe. (**c**) Enlarged area of EDS spectrum from Figure 5b to illustrate that Mg is not statistically detectable at this count rate. (**d** and **e**) Transmission electron microscope 2-D images of magnetite produced via the thermal decomposition of Fe-Mg carbonate globules (i.e., heated to 550 °C). Many of the crystals are euhedral with hexagonal or octagonal 2-D shapes (arrows in e). Note the rounded corners of magnetite in 5d (arrows) that are probably caused by a "roughening" effect during heating (i.e., 550 °C). (**f**) EDS scan of magnetite crystal in 5d (top arrow) that shows the crystal is free of Mg at 4000 total counts for Fe.

tion of Fe-rich carbonate (Golden et al. 2001). The thermal decomposition of Fe-rich carbonate to magnetite resulted in the formation of void space. We did not quantify the proportion of void space, but ~50% is expected on the basis of the difference between the density of siderite and magnetite [3.9 and 5.2 g/cm^3, respectively (Johnson and Olhoeft 1984)] assuming that there are no post-decomposition processes to compact, extend, or translocate void spaces.

Properties of hydrothermally precipitated magnetite (150 °C)

Magnetite crystals that co-precipitated with carbonate resulting from partial oxidation of Fe^{2+} during the hydrothermal precipitation of Fe-rich carbonate are often embedded in the carbonate matrix. Although the precipitated magnetite crystals formed in Fe-Mg solutions, they are chemically pure by EDS measurements to an Mg-detection limit of ~0.3 wt% (Figs. 5b and 5c). For the experiments starting with 2 mol% Mg solutions, only ~1% of the total number of magnetite crystals formed by precipitation from hydrothermal solutions (see discussion below). The morphology of precipitated magnetite crystals ranges from cubes to [111]-elongated crystals on the basis of tilt images. Their apices and edges are sharp (Fig. 5a), in contrast to the more rounded apices and edges produced by thermal decomposition of Fe-rich carbonate (Figs. 5d and 5e). The average crystal size and its standard deviation (a measure of the width of the size distribution) for precipitated magnetite crystals are significantly larger than those from our thermally decomposed magnetite crystals, the magnetite crystals obtained from the ALH84001 carbonate globules, and the magnetite crystals from MV-1 (Table 1). The only exception is the length dimension for whiskers formed by thermal decomposition of Fe-rich carbonate.

Properties of magnetite formed via thermal decomposition of Fe-rich carbonate

Most magnetite crystals formed by thermal decomposition of Fe-rich carbonate have rounded edges (Figs. 5d and 5e), which likely formed upon heating (i.e., a roughening effect) well below their melting temperature (Wortis 1988). Rounded edges may complicate the differentiation between [111]-ECO and [111]-THO models, because the rounded edges can be interpreted as very narrow faces near the limit of resolution under the TEM (e.g., very narrow {110}; see discussion below).

From experiments where initial solutions contained 2 mol% Mg and excluding clusters of magnetite whiskers attached to each other in parallel (Fig. 6), we investigated 578 individual crystals. We found that 66% of magnetite crystals are elongated on the [111] axis, 4% are euhedral without such elongation (e.g.,

TABLE 1. Size data for inorganic, biogenic (MV-1), and ALH84001 magnetite crystals

		Length (nm)		Width (nm)		Aspect ratio	
	Number*	Avg(SD)	Range	Avg(SD)	Range	Avg(SD)	Range
Inorganic magnetite from hydrothermal precipitation†							
All shapes	78	161(160)	14–900	125(128)	12–675	0.8(0.1)	0.5–1.0
Inorganic magnetite from siderite thermal decomposition†							
All shapes	578	50(20)	10–202	35(15)	6–134	0.7(0.1)	0.7–1.0
[111]-elongated‡	382	52(19)	10–148	35(14)	8–134	0.7(0.1)	0.4–1.0
Whiskers§	101	193(90)	52–481	36(13)	5–71	0.2(0.1)	0.0–0.3
Biogenic magnetite from MV-1							
[111]-elongated†	203	48(10)	20–64	34(7)	14–47	0.7(0.1)	0.5–1.0
[111]-elongated‖	206	42±13	6–69	30±9	6–46	0.7±0.1	0.5–1.0
[111]-elongated#	89	53	21–74	35	12–54	0.7	
[111]-elongated**	175	52	17–62			0.7	0.5–0.9
Martian meteorite ALH84001 carbonate globules							
[111]-elongated ‖	164	39±16	18–89	27±11	11–71	0.7±0.1	0.4–0.9

Note: SD = Standard Deviation.
* Number of magnetite crystals analyzed having a particular shape.
† This study.
‡ All [111]-elongated crystal shapes ([111]-THO, [111]-ECO, and [111]-ESO).
§ All elongated shapes with W/L <0.3.
‖ Thomas-Keprta et al. (2000).
Sparks et al. (1990) as cited in Thomas-Keprta et al. (2000).
** Calculated from Devouard et al. (1998).

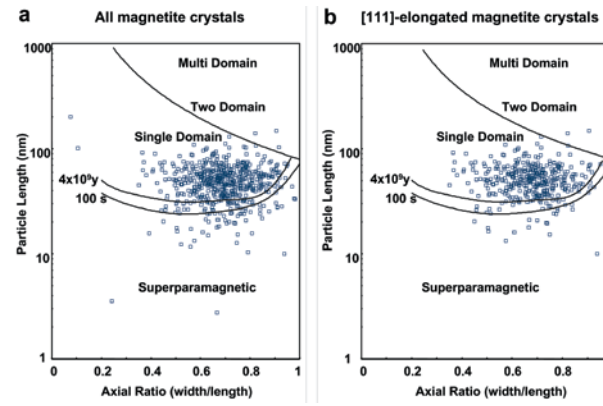

FIGURE 7. Plots of length vs. axial ratio (width/length) for **(a)** all inorganic magnetite crystals regardless of shape that were obtained from the thermal decomposition of Fe-rich carbonate and (**b**) inorganic magnetite crystals with elongation in the [111] direction. In both cases, the magnetite crystals strongly cluster in the single-domain region. The boundaries for the magnetic domains are from Butler and Banerjee (1975). The 100 s and 4×10^9 y curves represent the critical relaxation time boundaries for prismatic magnetite crystals at 290 K.

octahedral, cubic, platy), 2% are individual whiskers, and 28% have other irregular shapes (e.g., subhedral and anhedral crystals). Detailed morphological analysis for the [111]-elongated crystals follows. The whisker-shaped magnetite crystals (Fig. 6) are similar to those in ALH84001 described by Bradley et al. (1996), who suggested that the whisker-shaped magnetite grew from a vapor phase. We show here that whisker-shaped magnetite can form via the thermal decomposition of Fe-rich carbonate. Similar magnetite morphologies were observed for magnetite that formed from the thermal decomposition of siderite produced from high Mg starting solutions (i.e., 75 mol% Mg).

Figure 7 shows lengths vs. aspect ratios for magnetite crystals formed in our thermal decomposition experiments for both the full suite of crystals (Fig. 7a) and only the [111]-elongated crystals (Fig. 7b). Also shown are boundaries between magnetic domains (Butler and Banerjee 1975). The synthetic magnetite crystals, especially the [111]-elongated crystals, lie within or near the single magnetic domain size range. The distribution of our synthetic [111]-elongated magnetite crystals in Figure 7b is nearly identical to that for the purported biogenic subpopulation of [111]-elongated magnetite crystals in ALH84001 (see Fig. 10b in Thomas-Keprta et al. 2000).

The chemical purity of the magnetite crystals in ALH84001 is a key issue for their putative biogenicity, so it is important to document the compositions of our synthetic magnetite crystals. In our experiments, Mg was the only abundant element that can substitute significantly into magnetite (Mg^{2+} for Fe^{2+}). Magnetite crystals that formed from the Mg-poor siderites (original starting solutions containing 2 mol% Mg) contained no detectable Mg, i.e., <0.3 wt% by EDS (e.g., Fig. 5f). Many of the magnetite crystals that formed from siderite, which precipitated from high-Mg starting solutions (i.e., 75 mol% Mg), did contain detectable Mg (i.e., Mg content >0.3 wt%), although some crystals contained no detectable Mg. It is not unexpected that we can form Fe-pure magnetite via the thermal decomposition of Fe-carbonates that have formed in mixed Fe-Mg solutions. Woods and Garrels (1992) and Golden et al. (2000a) have shown that Fe-rich carbonate forms first in Mg-Fe mixed-carbonate hydrothermal systems. The Fe-rich carbonate is very pure in the central region of the globule; therefore, we expect to form chemically pure magnetite in such a mixed carbonate system.

Morphology of [111]-elongated magnetite crystals

As discussed above (Fig. 3b), the projection down a $\{110\}_c$ axis provides the best 2-D view for distinguishing among the [111]-elongated magnetite crystal shapes. Tilted image sequences are discussed below for 14 representative synthetic [111]-elongated magnetite crystals. These selected crystals have no detect-

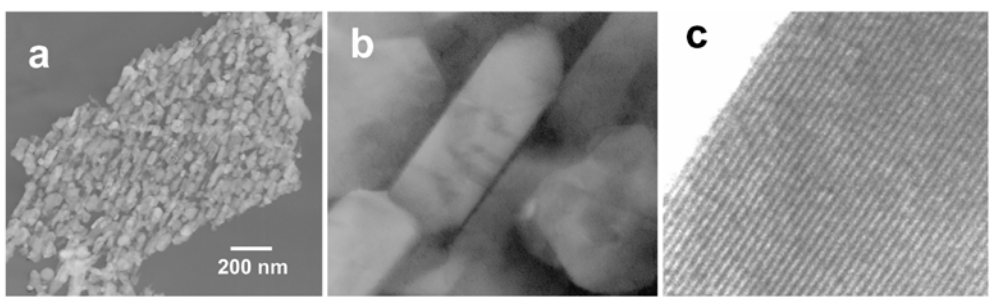

FIGURE 6. TEM images of a "raft" of oriented magnetite whiskers produced by the thermal decomposition of Fe-rich carbonate. (**a**) Full raft. (**b**) Enlarged view of individual magnetite whiskers from Figure 6a. (**c**) High resolution TEM lattice fringes of a magnetite whisker [(111) lattice fringes are ~0.48 nm].

able Mg and so are comparable in purity to those reported by Thomas-Keprta et al. (2000) from ALH84001. First, we present four crystals in orientations that are not views down a $\{110\}_e$ axis, in order to demonstrate that these views cannot be assigned unambiguously to either [111]-THO or [111]-ECO shapes. Then, we show ten other crystals that are views down a $\{110\}_e$ axis, and show that their projections are consistent with a [111]-ECO shape and not a [111]-THO shape.

Crysta1 1. The 2-D outlines of this magnetite crystal (Fig. 8) can be readily interpreted as either a [111]-THO or [111]-ECO shape. The crystal is viewed down a [$\bar{1}$12] zone axis at the +6°

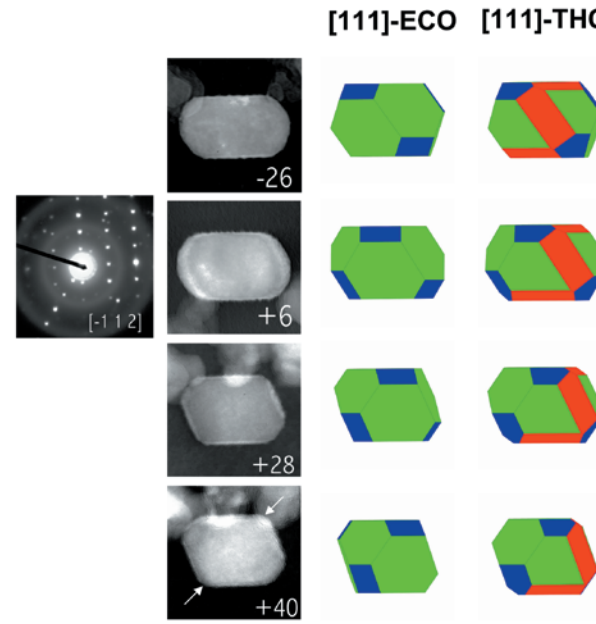

FIGURE 8. TEM tilt-sequence images of inorganic magnetite (Crystal 1) produced via the thermal decomposition of Fe-rich carbonate. The selected area electron-diffraction pattern at +6° tilt step corresponds to the [$\bar{1}$12] zone axis. Note the close fit of the [111]-THO shape and also of the [111]-ECO shape to the 2-D TEM images. The smooth curved edges and corners of the magnetite crystal in the TEM image makes it difficult to discern the break in outline continuity due to small faces. However, a pair of small {110} faces might be weakly expressed at the arrow marks in the +40° view [crystal length = 80 nm, width/length = 0.79; green = {111}, blue = {100}, and red = {110}].

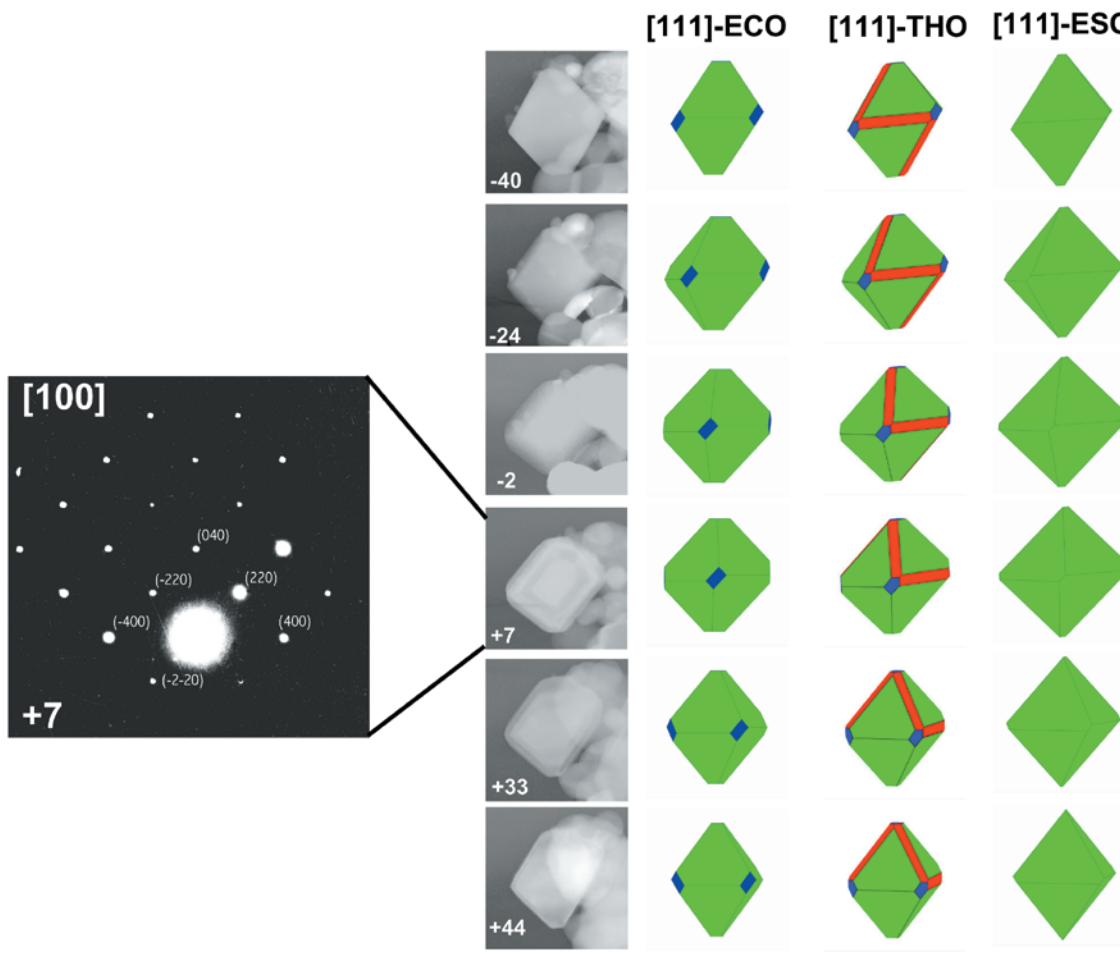

FIGURE 9. TEM tilt-sequence images of inorganic magnetite (Crystal 2) produced via the thermal decomposition of Fe-rich carbonate. Note the {100} truncations at +7° tilt; however, {110} faces are not expressed in any of these tilt images. Both the [111]-ECO and [111]-ESO models provide satisfactory fits to this tilt-image series [crystal length = 85 nm, width/length = 0.84; green = {111}, blue = {100}, and red = {110}].

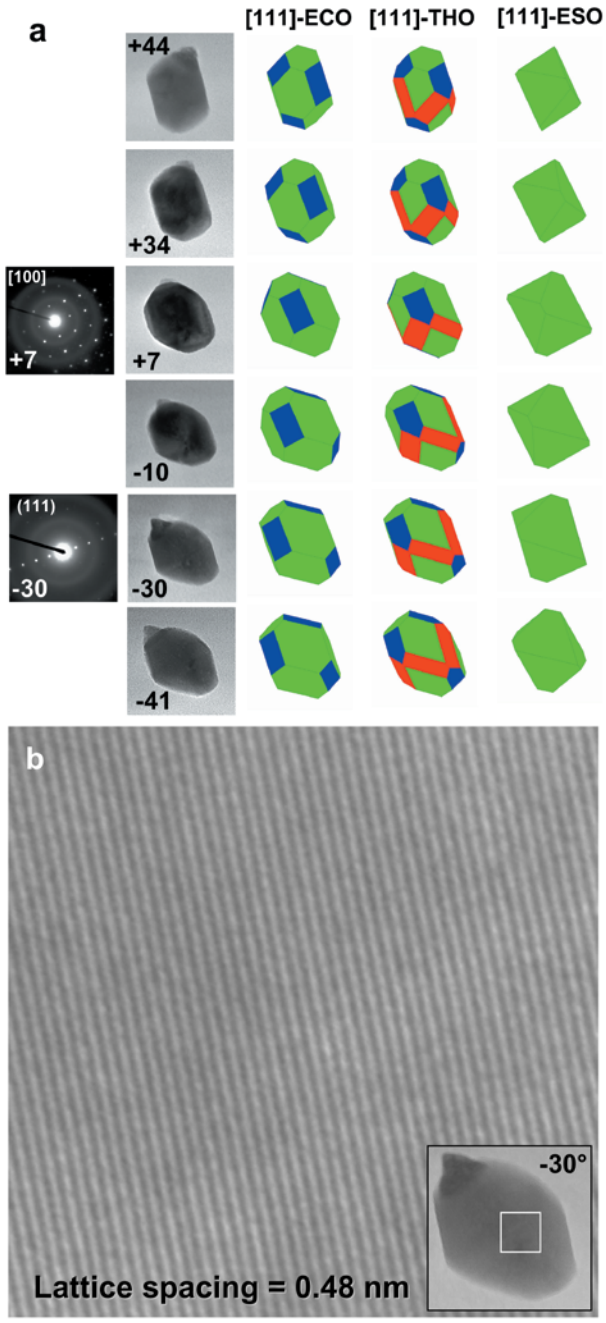

FIGURE 10. TEM images of inorganic magnetite (Crystal 3) produced via the thermal decomposition of Fe-rich carbonate. **(a)** TEM tilt sequence for synthetic magnetite crystal. Note the close fit of the [111]-THO and [111]-ECO models to the 2-D TEM images [crystal length = 67 nm, width/length = 0.75; green = {111}, blue = {100}, and red = {110}]. **(b)** High-resolution TEM image of crystal showing defect-free crystal lattice. Area of lattice fringes is shown on the crystal in the inset (the protrusion in the upper left corner of the crystal is an artifact from an adhering particle). Magnesium is not detectable in this particle by energy dispersive X-ray spectroscopy at 4000 counts for Fe and at 10 000 counts for multiple particles (data not shown).

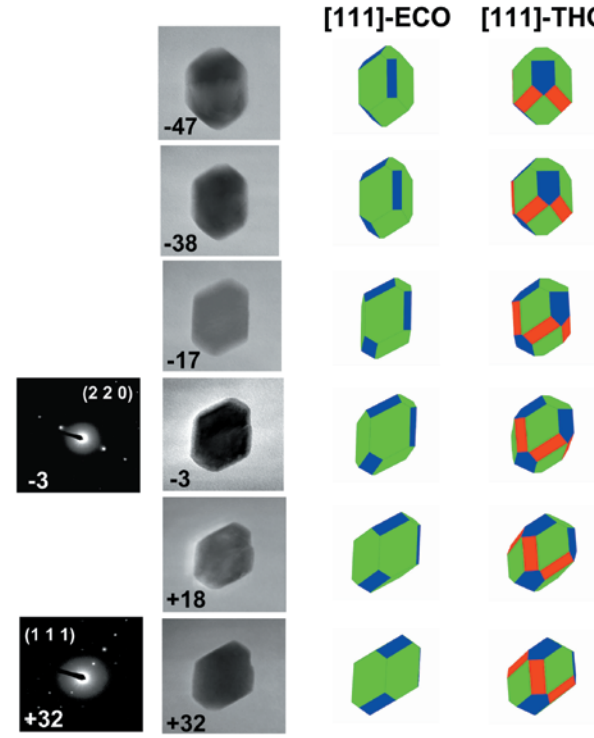

FIGURE 11. TEM tilt-sequence images of inorganic magnetite (Crystal 4) produced via the thermal decomposition of Fe-rich carbonate. Note that the [111]-THO and [111]-ECO models are not distinguishable in this tilt sequence [crystal length = 75 nm, width/length = 0.72; green = {111}, blue = {100}, and red = {110}].

rotation step and very close to a [011] zone axis at +40° rotation (the [011] orientation is consistent with the interfacial angles ({111}^{111}= 110° or 70° of the crystal projection at +40 position). In this view, the {100} truncations are obvious. The presence of {110} faces, needed to distinguish between [111]-THO and [111]-ECO shapes, cannot be established unambiguously. The faceted edge at +40° tilt position in the [111]-THO model (arrows in Fig. 8) does appear to fit the observed 2-D image if the {110} faces are very narrow. However, the edges of the magnetite crystal are rounded so that (within the image resolution) one cannot tell whether a {110} face is actually present.

Crystal 2. The second magnetite crystal (Fig. 9) was imaged over a tilt range of 84°. At -40° rotation, the outline of the crystal is a hexagon, bounded by four {111} and two {100} faces. At +7° rotation, the crystal is viewed down a {100} zone axis (confirmed by SAED); this view clearly shows {010} and {100} faces formed by truncations at its corners. The 2-D projections for this tilt sequence are insensitive to the presence or absence of the {110}, so that the [111]-THO and [111]-ECO models fit equally well.

Crystal 3. This crystal (Fig. 10), shown through an 85° tilt sequence, has outlines that are consistent with both [111]-THO and [111]-ECO shapes, but not the [111]-ESO shape. At a rotation of +7°, the SAED pattern indicates a view down a [100] zone axis; the view at –30° is along a (111) plane. The presence or the absence of {110} faces in this tilt sequence makes little dif-

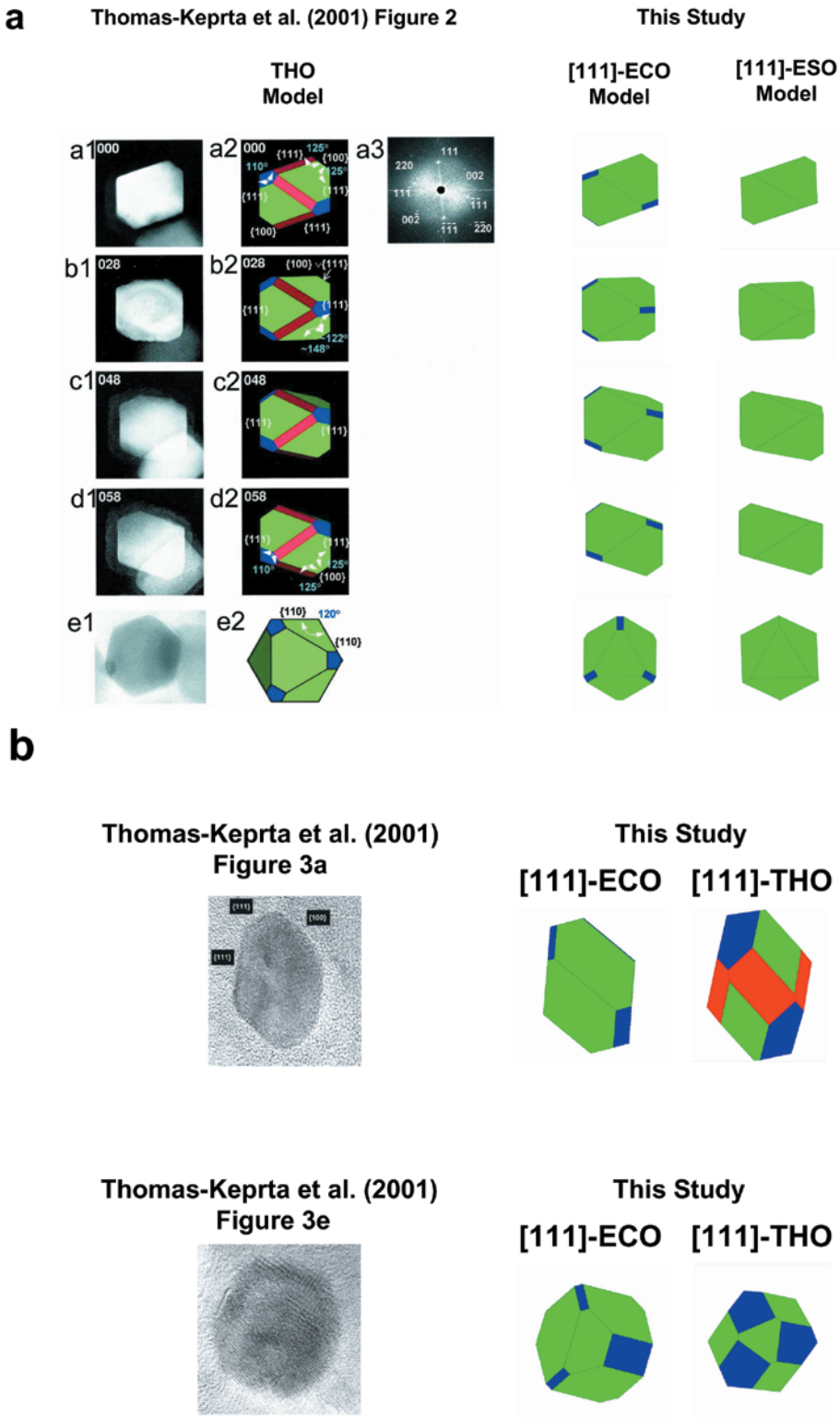

FIGURE 12. The [111]-THO, [111]-ECO and [111]-ESO models are shown for TEM images of magnetite crystals published by Thomas-Keprta et al. (2001). **(a)** TEM tilt-sequence images of a MV-1 magnetite crystal. Note the excellent agreement of the [111]-ECO model to the observed 2-D TEM images at all tilt positions. **(b)** TEM images of a magnetite crystal from Martian meteorite ALH84001. Again, note the excellent fit of the [111]-ECO model to these TEM 2-D image outlines. [Published with permission from the National Academy of Sciences, U.S.A.; see Thomas-Keprta et al. (2001).]

ference in the crystal outlines of a [111]-THO shape with {110} faces or a [111]-ECO model without {110} faces. The [111]-ESO shape is not reasonable for this crystal because {100} faces are clearly present (at +7°) in the tilt sequence. The HRTEM image shown in Figure 10b indicates that this crystal is free of lattice defects. All of the inorganic crystals presented here are free of lattice defects.

Crystal 4. The tilt sequence for the crystal in Figure 11 is

consistent with both the [111]-THO and [111]-ECO models. The two planes (220) and (111) observed in the SAED patterns are consistent with the assigned crystal orientation.

Summary of ambiguous shapes. These four examples are typical of inorganic magnetite crystals formed in our experiments by thermal decomposition of Fe-rich carbonate when the orientation is not down a $\{110\}_e$ axis: the [111]-THO and [111]-ECO models both fit the 2-D crystal projections equally well. We expect that it will be equally difficult to differentiate the [111]-THO and [111]-ECO models for ALH84001 and MV-1 magnetite crystals that are not oriented down a $\{110\}_e$ axis. For purposes of illustration, the THO model for ALH84001 and MV-1 magnetite crystals previously published (Thomas-Keprta et al. 2001) is compared to the [111]-ECO model in Figure 12. The MV-1 (Fig. 12a) and ALH84001 (Fig. 12b) magnetite crystals are described by either the [111]-THO or [111]-ECO models; hence, the orientations of these crystals prevent an unambiguous assignment to one of these models.

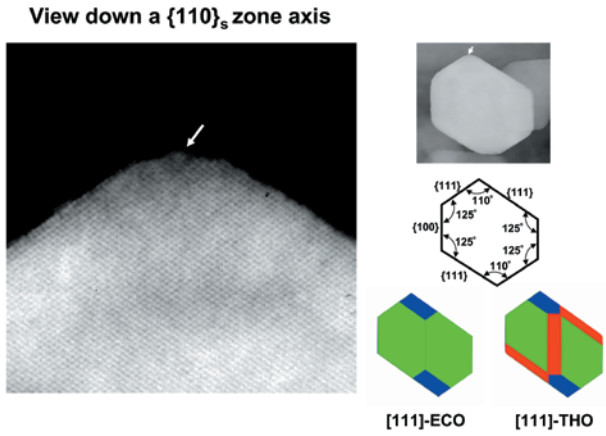

Figure 13. TEM images and morphological 3-D models looking down a $[110]_s$ axis ($\{110\}\cdot[111] = 0$) of an inorganically produced, elongated magnetite crystal (hexagonal outline) formed via the thermal decomposition of Fe-rich carbonate. Note the perfect crystal structure in the high-resolution TEM image and the rounding at the crystal edges in both TEM images that probably results from the "roughening" effect from heating to 550 °C [green = {111}, blue = {100}, and red = {110}]. The corner of the crystal is hidden at the bottom by another crystal.

Edge rounding. As noted above, many magnetite crystals appear to have rounded edges, which are possibly a manifestation of narrow {110} faces. That is, a [111]-ECO crystal with rounded edges can be interpreted as a [111]-THO crystal with narrow {110} faces (and vice versa). This ambiguity arises because a [111]-THO shape with {110} faces of zero width is a [111]-ECO shape. This ambiguity even extends to views in the $\{110\}_e$ projection, the most diagnostic view. Figure 13 shows an example of a rounded edge. That image is a view down a $\{110\}_s$ zone axis perpendicular to the [111] elongation axis. The [111]-THO and [111]-ECO models do not have {110} faces expressed in this orientation (see models in Fig. 13); hence, this edge must be considered as rounded.

Crystal 5 ($\{110\}_e$ oriented). Figure 14 shows an inorganic magnetite from one of our experiments, tilted through a $\{110\}_e$

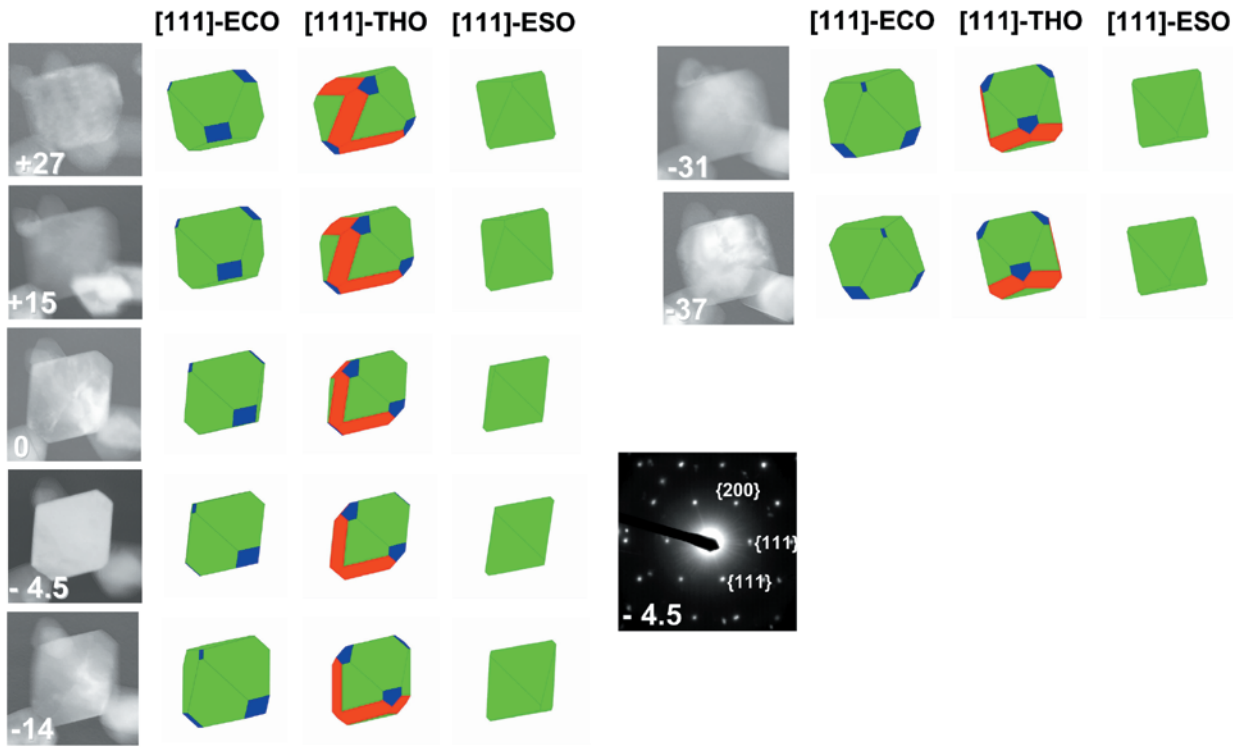

FIGURE 14. TEM tilt-sequence images of an inorganic magnetite (Crystal 5) produced via the thermal decomposition of Fe-rich carbonate. The –4.5° tilt step has the crystal oriented looking down the $\{110\}_e$ axis (see Fig. 3). Note that the 2-D TEM crystal image fits the [111]-ECO model and not the [111]-THO model. The weakly expressed spots are due to diffraction from other crystals in the field of view [crystal length = 65 nm, width/length = 0.86; green = {111}, blue = {100}, and red = {110}].

axis orientation at –4.5° tilt, as confirmed by the SAED pattern. The 2-D projection at the $\{110\}_e$ axis orientation is a hexagon, representing four {111} faces and two {100} faces of the [111]-ECO model. If the crystal were a [111]-THO shape, it would have {110} faces, which are not discernible. Although some rounded edges could possibly be interpreted as manifestations of very narrow {110} faces, other edges are also rounded. Therefore, we infer that the grain lacks {110} faces and is thus [111]-ECO.

Crystals 6 through 14 ($\{110\}_e$ oriented). The magnetite crystal just discussed and nine others from our experiments are shown in a $\{110\}_e$ axis orientation in Figure 15. All 10 crystals are consistent only with a [111]-ECO shape. The $\{110\}_e$ orientation for all crystals was confirmed by 2D-FFT, as shown for the top crystal in the figure. Image tilt sequences show that these crystals are all elongated along [111]. These 10 representative and randomly selected crystals show that the [111]-ECO shape is the most common [111]-elongated morphology for our inorganic magnetite crystals. For later comparison with [111]-elongated crystals from ALH84001 and MV-1, we note again that the inorganic [111]-ECO crystals described above contain Mg below detection, and have width/length ratios of 0.6-0.9.

Comparison of biogenic, inorganic, and ALH84001 [111]-elongated magnetite crystals

The critical part of this study is the comparison of nanophase magnetite crystals in the ALH84001 meteorite, those produced by the MV-1 bacterium, and the inorganic, abiogenic magnetite produced in our experiments. We have found that the MV-1 population is distinct, both in crystal morphology and in regularity of shape, from those in both ALH84001 and our experiments.

There is no question that the magnetite populations in experimental, meteorite, and MV-1 samples are similar in many respects. All three populations have sizes and shapes (Table 1) that imply behavior as magnetic single-domain particles. Magnetite crystals from all three types of samples are essentially pure Fe oxide (without detectable Mg or other impurities) and contain few or no crystal structural flaws, except for spinel-law twins. Thomas-Keprta et al. (2001, 2002) have called on the similarity between the MV-1 and the meteorite magnetite crystals as "presumptive biosignatures" of ancient life on Mars.

The primary, if not the exclusive, factor that differentiates the experimental, meteorite, and MV-1 magnetite populations is crystal morphology (i.e., [111]-ECO vs. [111]-THO vs. [111]-ESO). We found that the three populations are not dominated by the same [111]-elongated shape (Fig. 16). MV-1 magnetite crystals are dominantly [111]-THO, and those from both ALH84001 and our inorganic experiments are dominantly [111]-ECO. In addition, we found that the magnetite crystals from MV-1 are distinctly more regular in crystal form than those from either ALH84001 or our experiments. Next, we discuss comparisons of crystal shape and regularity of shape in more detail.

What shape are the [111]-elongated crystals?

For biogenic magnetite from MV-1, the widths of the {110} faces are well expressed (arrow in $\{110\}_e$ image of Fig. 16a). We analyzed 25 MV-1 crystals in the $\{110\}_e$ axis orientation and 18 of them had similar well-defined faces (rounded edges were not counted as faces). Therefore, and in agreement with Clemett et al. (2002), the predominant crystal morphology for MV-1 magnetite is clearly [111]-THO and not [111]-ECO.

For our synthetic inorganic magnetite crystals, rounded edges are present at the locations of the well-developed {110} faces in MV-1 (see arrow in the $\{110\}_e$ image of Fig. 16b). As discussed in the last section, this edge rounding is intrinsic and does not result from {110} faces too narrow to be resolved, so that the crystal morphology is [111]-ECO. In any case, the morphology of the inorganic crystals is clearly different from that of biogenic MV-1 crystals (i.e., rounded edges vs. well-developed faces).

For ALH84001 magnetite crystals examined in this study with a $\{110\}_e$ axis orientation (6 total crystals), the locations of the well-developed {110} faces in MV-1 are (like our inorganic magnetite crystals) typically characterized by rounded edges (arrow in the $\{110\}_e$ image of Fig. 16c). Again, because of evidence for intrinsic edge rounding in the inorganic magnetite (Fig. 16b), we interpret the shape as [111]-ECO. Note that the degree of edge rounding is less in the ALH84001 magnetite crystals than in our inorganic crystals (see arrows in the $\{110\}_e$ axis images of Figs. 16b and 16c), so that ALH84001 crystals correspond better to the ideal [111] -ECO shape than do our inorganic crystals. The shapes of synthetic and ALH84001 magnetite crystals are identical and neither is similar to the shape of MV-1 magnetite crystals.

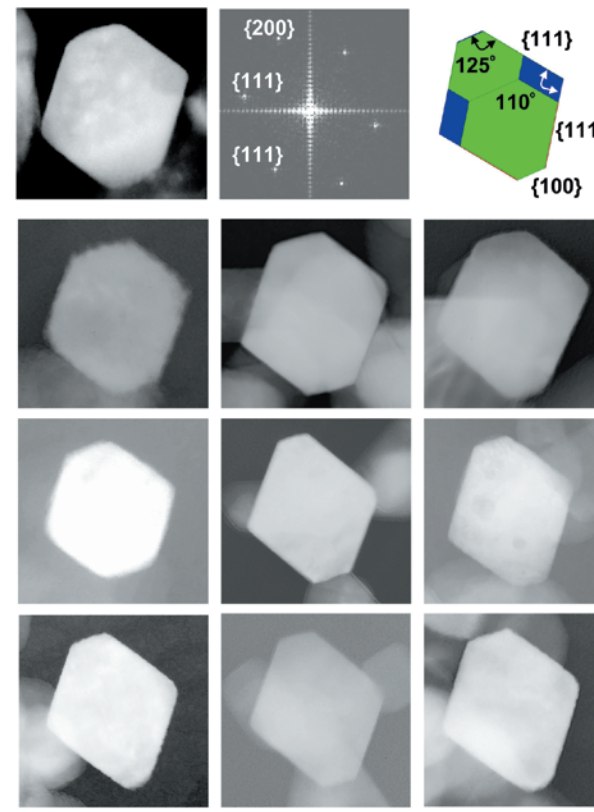

Figure 15. TEM images of ten individual inorganic magnetite crystals (Crystals 6-14) produced via the thermal decomposition of Fe-rich carbonate. These crystals are all oriented looking down a $\{110\}_e$ axis, which clearly illustrate that these crystals are best fitted by the [111]-ECO morphological model shown here [green = {111} and blue = {100}]. A 2-D fast Fourier transformation of the lattice fringes is shown for the uppermost crystal.

Thomas-Keprta et al. (2001) assigned the [111]-THO shape to the [111] elongated crystals in ALH84001. Their model representation is shown in Figure 16d (b2), and it has narrow {110} faces. We argue that Thomas-Keprta et al. (2001) interpreted the intrinsically rounded edges as narrow faces and that the crystal shape is actually [111]-ECO with intrinsically rounded edges. In any case, the ALH84001 crystal shape as observed by us (see $\{110\}_e$ axis image of Fig. 16c) and by Thomas-Keprta et al. (2001) (see the $\{110\}_e$ axis image of Fig. 16d) is clearly different from the crystal shape commonly observed for MV-1 by us (see $\{110\}_e$ axis image of Fig. 16a).

In our TEM mounts of ALH84001 magnetite crystals, we found only 6 out of 222 magnetite crystals (~3%) were oriented in the $\{110\}_e$ direction. All six had the [111]-ECO shape. The other 216 crystals were elongated, but the elongation direction was not determined. Presumably, the percentage of [111]-ECO crystals is actually higher because we analyzed only crystals that had the $\{110\}_e$ orientation independent of shape (i.e., [111]-THO, [111]-ECO, and [111]-ESO).

About 27% of the magnetite crystals in ALH84001 carbonate globules are [111]-elongated (Thomas-Keprta et al. 2000, 2001, 2002). However, they reported bright-field TEM images in the $\{110\}_e$ orientation for at most 5 magnetite crystals, and we interpret those images as representing the [111]-ECO shape. Therefore, in our view, all magnetite crystals from the ALH84001 meteorite that have been analyzed by bright-field

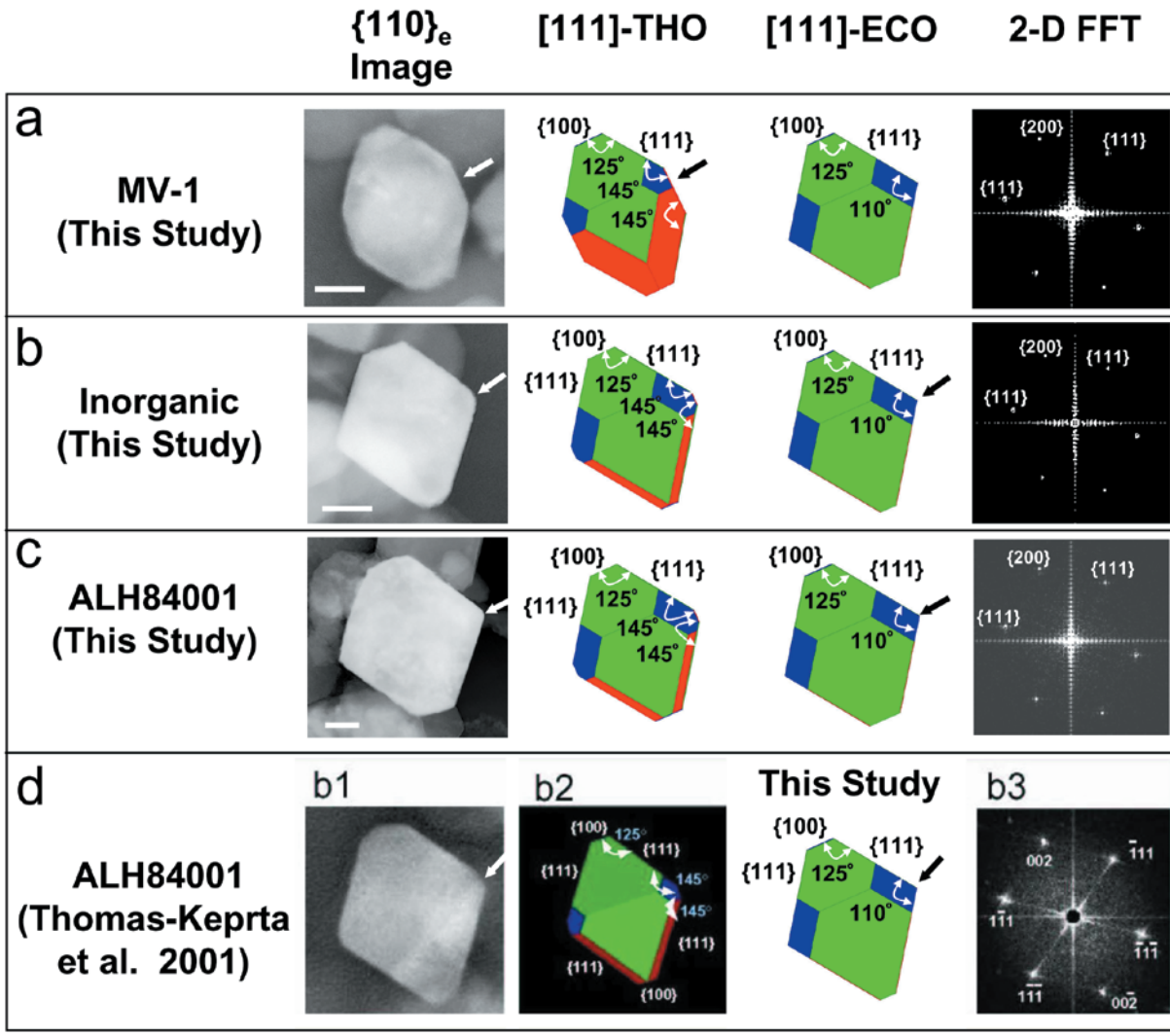

FIGURE 16. TEM images looking down a $\{110\}_e$ axis for the most common [111]-elongated morphological forms of (**a**) magnetotactic bacterial strain MV-1, (**b**) inorganic magnetite formed via the thermal decomposition of Fe-rich carbonate, and (**c** and **d**) subpopulation of magnetite crystals in Martian meteorite ALH84001. MV-1 magnetite crystals have well-defined {110} faces (arrow in **a**) that best fit the [111]-THO model. Inorganic magnetite did not have well-defined {110} faces (arrow in **b**) and best fit the [111]-ECO morphology. ALH84001 magnetite morphology was very similar to the inorganic magnetite and best fits the [111]-ECO model. The crystal in **d** from the published works of Thomas-Keprta et al. (2001) is shown for comparison with our results in **c**. This crystal does not have well-defined {110} faces (arrow in d) and best fits the [110]-ECO model [2-D FFT = 2-D fast Fourier transformation of lattice fringes, green = {111} faces, blue = {100} faces, and red = {110} faces; bar = 20 nm]. [Fig. 16d Published with permission from the National Academy of Sciences, U.S.A.; see Thomas-Keprta et al. (2001).]

TEM in the $\{110\}_e$ orientation have the [111]-ECO shape. In any case, the percentage of [111]-elongated crystals in ALH84001 is between 3% and 27%. These disparate values may reflect the spatial heterogeneity of [111]-elongated magnetite crystals within ALH84001 carbonate globules.

How regular are the [111]-elongated magnetite crystals?

The crystals of synthetic and MV-1 magnetite shown in Figure 16 are representative of the majority of magnetite crystals and are particularly symmetric in their 2-D views. However, deviations from symmetric crystals (i.e., asymmetric growth in multiple directions) are occasionally present in populations of both synthetic and MV-1 magnetite.

Figure 17a illustrates synthetic magnetite crystals whose shapes are [111]-THO, [111]-ECO, and [111]-ESO, or combinations of those shapes. For example, the topmost crystal in Figure 17a has well-developed {110} faces consistent with the [111]-THO model. The next synthetic crystal in Figure 17a shows a well-developed {110} face consistent with [111]-THO shape on one side and no face on the opposite side consistent with the [111]-ECO shape. Similar shapes have been reported for elongated ALH84001 magnetite crystals (see Figs. 4a through 4c of Thomas-Keprta et al. 2002). The lowermost crystal in Figure 17a shows a synthetic magnetite crystal with a shape close to [111]-ESO.

Figure 17b shows ranges of crystal shapes that we observed for MV-1 magnetite. Note the variation in the range of the width of {110} faces (red arrows) and {100} faces (blue arrows). The shape of the lowermost MV-1 crystal in Figure 17b is best characterized as [111]-ESO, which is identical to the inorganic magnetite shown in the lowermost crystal in Figure 17a. All MV-1 shapes are relatively more symmetrical than those for both synthetic and ALH84001 [111]-elongated magnetite crystals.

We emphasize that the crystals just discussed are not representative of the general population of magnetite crystals. For inorganic [111]-elongated magnetite crystals obtained from the thermal decomposition of hydrothermally precipitated Fe-rich carbonate and for [111]-elongated magnetite crystals obtained from our sample of ALH84001, the most common shape is [111]-ECO (see crystal outlined by red box in Fig. 17a). For biogenic magnetite crystals from MV-1, the most common shape is [111]-THO with well-developed {110} faces (see crystal outlined by red box in Fig. 17b). The difference in morphology of ALH84001 magnetite and MV-1 magnetite is in agreement with the findings of Buseck et al. (2001), who suggested that the morphology of magnetite from three bacterial strains including MV-1 differ, and that none of them uniquely matched those reported from the Martian meteorite ALH84001.

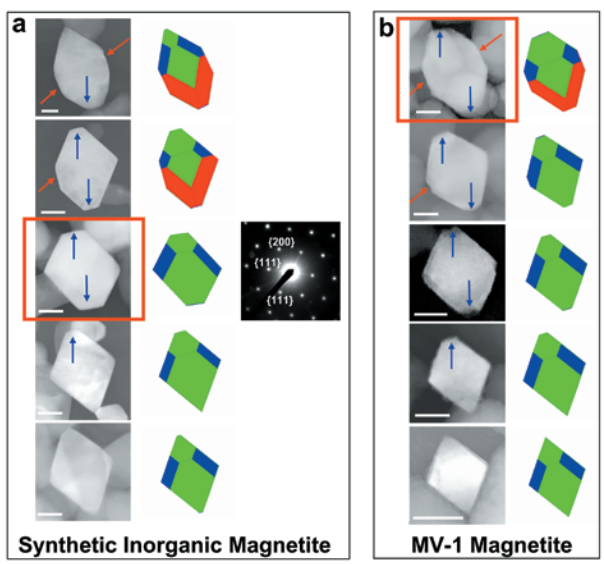

Figure 17. TEM images and best fit 3-D morphological models of magnetite crystals looking down the $\{110\}_e$ axis. These images illustrate variations in magnetite morphology. (**a**) Inorganic magnetite formed via the thermal decomposition of Fe-rich carbonate; (**b**) Biogenic magnetite produced by magnetotactic bacterial strain MV-1 [green = {111} faces, blue = {100} faces, and red = {110} faces; bar = 20 nm]. Images outlined in the red boxes represent the most characteristic morphology for each group of [111]-elongated crystals oriented down a $\{110\}_e$ axis.

Is biogneic magnetite present in Martian meteorite ALH84001?

Three lines of argument are critical to establishing whether some magnetite crystals in the ALH84001 meteorite (the [111]-elongated crystals) formed with or without biological intervention. First is to evaluate the claim of Thomas-Keprta et al. (2001, 2002) that the characteristics of these ALH84001 magnetite crystals are consistent with those produced by the bacterium MV-1. Second is whether these ALH84001 magnetite crystals could be similar to those formed by other types of life forms on Earth. Third is whether inorganic processes can produce the ALH84001 magnetite crystals.

Magnetite crystals from the magnetotactic bacterium MV-1 have been central to the debate about ALH84001 because this bacterium was singled out by Thomas-Keprta et al. (2001, 2002). Their claims about biogenicity of the ALH84001 magnetite refer only to the MV-1 bacterium. This and other studies of magnetosome magnetite crystals produced by MV-1 show that they are chemically pure, commonly free of crystalline defects, lie in the single-magnetic-domain size range (e.g., Bazylinski 1990; Bazylinski and Frankel 2000; Thomas-Keprta et al. 2000, 2001, 2002; Clemett et al. 2002), and are predominantly [111]-THO in morphology with characteristic {110} faces (e.g., Thomas-Keprta et al. 2001, 2002; Clemett et al. 2002).

Thomas-Keprta et al. (2001, 2002) argued that the [111]-elongated magnetite crystals from ALH84001 share all of these characteristics. We agree with Thomas-Keprta et al. (2001, 2002), except for the critical parameter of crystal morphology. Specifically, we demonstrated in detail that most MV-1 magnetosome magnetite crystals have [111]-THO shapes with well-developed {110} faces (see also Clemett et al. 2002). We also confirm the observations of Thomas-Keprta et al. (2000, 2001, 2002) for the physical shape of the ALH84001 magnetite, with a crucial difference. Thomas-Keprta et al. interpreted rounded edges on the ALH84001 [111]-elongated grains as representing very narrow faces (unresolved by TEM) in the $\{110\}_e$ zone, and thus interpret the grains as [111]-THO. We, on the other hand, note that most edges and vertices in the ALH84001 [111]-elongated crystals are rounded and ascribe all the rounding to growth conditions.

Thus, we interpret the ALH84001 magnetite crystals as [111]-ECO shapes with slightly rounded edges.

However, despite what name one wishes to apply to the crystals, we have shown that the shapes of MV-1 and ALH84001 [111]-elongated magnetite crystals are distinctly different—the former most commonly have well-developed {110} faces and the latter most commonly have rounded edges with no clear expression of {110} faces. Thus, the shape of the [111]-elongated magnetite crystals in ALH84001 is not identical to that from the bacterium MV-1. The claim that a subpopulation of magnetite crystals is biogenic in origin by analogy with MV-1 is not supported by these observations.

Our work does not prove that Mars is sterile, nor does it prove that the [111]-elongated magnetite crystals in ALH84001 are inorganic. Our work does show that inorganic processes can make the magnetite crystals in ALH84001, so any claim to biogenicity is equivocal. On Earth, magnetite crystals are produced by many varieties of bacteria (and other living things) in a wide range of morphologies, sizes, and structures (Taylor et al. 2001). It has not been shown to date, however, that magnetite crystals identical to those in ALH84001 are a product of terrestrial biological activity. It may be that some ancient Martian organism that has no known terrestrial counterpart produced magnetite crystals identical to those in ALH84001. However, our demonstration that an abiotic inorganic history can produce magnetite crystals like those in ALH84001 does not support an exclusively biogenic origin.

IMPLICATIONS

We have shown that the [111]-elongated magnetite crystals produced inorganically by the thermal decomposition of hydrothermally precipitated Fe-rich carbonate have all the defining characteristics of biogenic MV-1 magnetite except the crystal shape. These inorganically produced magnetite crystals are [111]-ECO forms with slightly rounded edges and vertices. The submicrometer magnetite crystals from the ALH84001 Martian meteorite are dominantly also this same [111]-ECO shape. On the basis of this correspondence in physical and chemical properties of magnetite crystals and the nature of precursor materials, we suggest that formation pathways also correspond: namely, the thermal decomposition of Fe-bearing carbonate minerals.

On the other hand, if one assumes (for the sake of argument) that the magnetite crystals in ALH84001 are biogenic in origin, and then it follows from our experiments that an inorganic process also can replicate those crystals. Consequently, the magnetite crystal morphology cannot be used as a biomarker and the morphologic argument for a biogenic origin cannot be applied unequivocally for ALH84001 magnetite crystals with [111] elongation.

Results of the investigations reported here show that it is unnecessary to invoke biogenic processes to explain formation of the [111]-elongated magnetite crystals in Martian meteorite ALH84001. Inorganic processes exclusively can account for the putative biogenic subfraction of [111]-elongated magnetite crystals in the meteorite. Furthermore, laboratory experiments also provide an inorganic process analogue for formation of magnetite in ALH84001, namely, precipitation of Fe-rich carbonates from circulating hydrothermal and carbonate-rich solutions and their subsequent thermal decomposition. Such decomposition may have been induced by heating associated with meteoritic impact or volcanic processes, to form the observed population of single domain, chemically pure, defect-free magnetic crystals that have a [111]-ECO shape with intrinsic edge and corner rounding as their most common morphology. Periclase formation as the thermal decomposition product of Mg-rich carbonate (e.g., Barber and Scott 2002) and formation of PAHs (McCollom 2003) are additional manifestations of the heating event. Finally, the morphology of MV-1 magnetite crystals ([111]-THO with well-developed {110} faces) remains a biomarker that is uncommon in our inorganic products and in Martian meteorite ALH84001.

ACKNOWLEDGMENTS

This work was supported by the NASA Exobiology program (NRA 99-OSS-01). We thank D.A. Bazylinski for samples of magnetotactic bacteria MV-1. The authors thank J.H. Jones, C.S. Romanek, D.H. Lindsley, and B.L. Jolliff for critical reviews of this manuscript and F. D. Bloss for critically reviewing an earlier version of the manuscript. LPI contribution no. 1201.

REFERENCES CITED

Barber, D.J. and Scott, E.R.D. (2002) Origin of supposedly biogenic magnetite in the Martian meteorite Allan Hills 84001. Proceedings of the National Academy of Science, 99, 6556–6561.

Bazylinski, D.A. (1990) Anaerobic production of single-domain magnetite by the marine, magnetotactic strain, MV-1. In R.B. Frankel and R.B. Blakemore, Eds., Iron Biominerals, p. 69–77. Plenum Press. New York.

Bazylinski, D.A. and Frankel, R.B. (2000) Biologically controlled mineralization of iron minerals by magnetotactic bacteria. In D.R. Lovely, Ed., Environmental microbe-metal interactions, p. 109–144. American Society of Microbiology Press, Washington, D.C.

Bradley, J.P., Harvey, R.P., and McSween, Jr. H.Y. (1996) Magnetite whiskers and platelets in the ALH84001 Martian meteorite: evidence of vapor phase growth. Geochimica et Cosmochimica Acta, 60, 5149–5155.

Bradley, J.P., McSween, H. Y., and Harvey, R.P. (1998) Epitaxial growth of nanophase magnetite in Martian meteorite ALH84001: Implications for biogenic mineralization. Meteoritics and Planetary Science, 33, 765–773.

Brearley, A.J. (1998) Magnetite in ALH84001: Product of decomposition of ferroan carbonate. Lunar and Planetary Science XXIX, Abstract no. 1451, CD-ROM.

Buseck, P.R., Dunnin-Borkovski, R.E., Devouard, B., Frankel, R.B., McCartney, M.R., Midgley, P.A., Posfai, M., and Weyland, M. (2001) Magnetite morphology and life on Mars. Proceedings of the National Academy of Science, 98, 13490–13495.

Butler R.F. and Banerjee S.K. (1975) Theoretical single-domain grain size range in magnetite and titanomagnetite. Journal of Geophysical Research 80, 4049–4058.

Catling, D.C. (1999) A chemical model for evaporates on early Mars: Possible sedimentary tracers of the early climate and implications for exploration. Journal of Geophysical Research, 104, 16453–16469.

Clemett, S.J., Thomas-Keprta, L.L., Shimmin, J.L., Morphew, M., McIntosh, J.R., Bazylinski, D.A., Kirshvink, J.L., Wentworth, S.J., McKay, D.S., Vali, H., Gibson, E.K., and Romanek, C.S. (2002) Crystal morphology of MV-1 magnetite. American Mineralogist, 87, 1727–1730.

Devouard, B., Posfai, M., Hua, X., Bazylinski, D.A., Frankel, R.B., and Buseck, P.R. (1998) Magnetite from magnetotactic bacteria: Size distribution and twinning. American Mineralogist, 83, 1387–1398.

Golden, D.C., Ming, D.W., Schwandt, C.S., Morris, R.V., Yang, S.V., and Lofgren, G.E. (2000a) An experimental study on kinetically driven precipitation of calcium-magnesium-iron carbonates from solution: Implications for the low-temperature formation of carbonates in Martian meteorite Allan Hills 84001. Meteoritics and Planetary Science, 35, 457–465.

Golden, D. C., Ming, D.W., Schwandt, C.S., Lauer, H.V., Socki, R.A., Morris, R.V., Lofgren, G.E., and McKay, G.A. (2000b) Inorganic formation of zoned Mg-Fe-Ca-carbonate globules with magnetite and sulfide rims similar to those in Martian meteorite ALH84001. Lunar and Planetary Science XXXI, Abstract no. 1799, CD-ROM.

Golden, D. C., Ming, D.W., Schwandt, C.S., Lauer, H.V., Socki, R.A., Morris, R.V., Lofgren, G.E., and McKay, G.A. (2001) A simple inorganic process for formation of carbonates, magnetite and sulfides in Martian meteorite ALH84001. American Mineralogist, 86, 370–375.

Golden, D. C., Ming, D.W., Schwandt, C.S., Lauer, H.V., Morris, R.V., Lofgren, G.E., and McKay, G.A. (2002) Inorganic formation of "Truncated hexa-octahedral" magnetite: Implications for inorganic processes in ALH84001 meteorite.

Lunar and Planetary Science XXXIII, Abstract no. 1839, CD-ROM.
Johnson, G.R. and Olhoeft, G.R. (1984) Densities of Rocks and Minerals. In R.S. Carmichael Ed., CRC Handbook of Physical Properties of Rocks, Volume III, p. 1–38, CRC Press, Inc., Boca Raton, Florida.
Joy, D.C., Romig, A.D., and Goldstein, J.I., Eds. (1986) Principles of analytical electron microscopy. Plenum Press, New York.
Koziol, A.M. and Brearly, A.J. (2002) A non-biological origin for the nanophase magnetite grains in ALH84001: Experimental Results. Lunar and Planetary Science XXXIII, Abstract no. 1672, CD-ROM.
Kring, D.A., Swindle, T.D., Gleason, J.D., and Grier, J.A. (1998) Formation and relative ages of maskelynite and carbonate in ALH84001. Geochimica et Cosmochimica Acta, 62, 2155–2166.
Mann, S., Sparks, N.H.C., and Blakemore, R.P. (1987) Ultrastructure and characterization of anisotropic magnetic inclusions, in magnetotactic bacteria. Proceedings of the Royal Society of London, 231, 469–476.
McKay D.S., Gibson, E.K. Jr., Thomas-Keprta, K.L., Vali, H., Romanek, C.S., Clemett, S.J., Chillier X.D.F., Maechling, C.R., and Zare, R.N. (1996) Search for past life on Mars: Possible relic biogenic activity in Martian meteorite ALH84001. Science, 273, 924–930.
McCollom, T.M. (2003) Formation of meteorite hydrocarbons from thermal decomposition of siderite ($FeCO_3$). Geochimica et Cosmochimica Acta, 67, 311–317.
Taylor, A.P., Barry, J.C., and Webb, R.I. (2001) Structural and morphological anomalies in magnetosomes: Possible biogenic origin for magnetite in ALH84001. Journal of Microscopy, 201, 84–106.
Thomas-Keprta, K.L., Bazylinski, D., Kirschvink, J.L., Clemett, S.J., McKay, D.S., Wentworth, S.J., Vali, H., Gibson, E.K., and Romanek, C.S. (2000) Elongated prismatic magnetite crystals in ALH84001 carbonate globules: Potential Martian magnetofossils. Geochimica et Cosmochimica Acta, 64, 4049–4081.
Thomas-Keprta, K.L., Clemett, S.J., Bazylinski, D.A., Kirschvink, J.L., McKay, D.S., Wentworth, S.J., Vali, H., Gibson, E.K., McKay, M.F., and Romanek, C.S. (2001) Truncated hexa-octahedral magnetite crystals in ALH84001: Presumptive biosignatures. Proceedings of the National Academy of Science, 98, 2164–2169.
Thomas-Keprta, K.L., Clemett, S.J., Bazylinski, D.A., Kirschvink, J.L., McKay, D.S., Wentworth, S.J., Vali, H., Gibson, E.K., and Romanek, C.S. (2002) Magnetofossils from ancient Mars: A robust biosignature in the Martian meteorite ALH84001. Applied and Environmental Microbiology, 68, 3663–3672.
Treiman, A.H. (1995) A petrographic history of Martian meteorite ALH84001: Two shocks and an ancient age. Meteoritics, 30, 294–302.
———(1998) The history of ALH84001 revised: Multiple shock events. Meteoritics and Planetary Science, 33, 753–764.
———(2001) A hypothesis for the abiotic and non-martian origins of putative signs of ancient Martian life in ALH84001. Lunar and Planetary Science XXXII, Abstract no. 1304, CD-ROM.
———(2003) Submicron magnetite grains and carbon compounds in Martian meteorite ALH84001: Inorganic abiotic formation by shock and thermal metamorphism. Astrobiology, 3, 369–392.
Treiman, A.H. and Keller, L.P. (2000) Magnetite bearing layers in Allan Hills 84001 carbonate globules: Bulk and mineral compositions. Meteoritics and Planetary Science, 35, A158–159.
Weber, S. (2000) JCrystal (Ver. 1.02): A crystal Morphology Editor and Viewer. JCrystalSoft, http://www.jcrystal.com. 3550 Pacific Ave., no. 311, Livermore, California.
Woods, T.L. and Garrels, R.M. (1992) Calculated aqueous-solution-solid solution relations in the low-temperature system CaO-MgO-FeO-CO_2-H_2O. Geochimica et Cosmochimica Acta, 56, 3031–3043.
Wortis, M. (1988) Equilibrium crystal shapes and interfacial phase transitions. In R. Vanselow and R.F. Howe, Eds., Chemistry and physics of solid surfaces VII, p. 367–405, Springer Verlag, New York.

MANUSCRIPT RECEIVED JULY 9, 2003
MANUSCRIPT ACCEPTED JANUARY 25, 2004
MANUSCRIPT HANDLED BY BRAD JOLLIFF